J. Electrochem. Sci. Eng. **14(3)** (2024) 275-296; http://dx.doi.org/10.5599/jese.2177

Open Access : : ISSN 1847-9286
www.jESE-online.org

Original scientific paper

Inhibition performance of a novel quinoxaline derivative for carbon steel corrosion in 1 M HCl

Latifa Chahir[1], Fouad Benhiba[1,2], Nadeem Abad[3], Hassan Zarrok[4], Ismail Warad[5], Mousa Al-Noaimi[6], Driss Benmessaoud Left[7], Mustapha Zertoubi[7], Mustapha Allali[8], Abdelkebir Bellaouchou[1], Youssef Ramli[3,9] and Abdelkader Zarrouk[1,✉]

[1]*Laboratory of Materials, Nanotechnology and Environment, Faculty of Sciences, Mohammed V University in Rabat, Av. Ibn Battouta, P.O. Box. 1014 Agdal-Rabat, Morocco*
[2]*Higher Institute of Nursing Professions and Health Techniques of Agadir Annex Guelmim, Guelmim, Morocco*
[3]*Laboratory of Medicinal Chemistry, Drug Sciences Research Center, Faculty of Medicine and Pharmacy, Mohammed V University, Rabat, Morocco*
[4]*Laboratory of Advanced Materials and Process Engineering, Faculty of Sciences, Ibn Tofail University, P.O. Box. 133, 14000, Kenitra, Morocco*
[5]*Department of Chemistry, AN-Najah National University, P.O. Box 7, Nablus, Palestine*
[6]*Chemistry Department, Faculty of Science, Kuwait University, P.O. Box 5969, Safat 13060, Kuwait*
[7]*Laboratoire Interface Matériaux Environnement (LIME), Faculty of Sciences Ain Chock University Hassan II, Casablanca, B.P 5366, Morocco*
[8]*Institute of Nursing Professions and Health Techniques Fez, EL Ghassani Hospital, Fez 30000, Morocco*
[9]*Mohammed VI Center for Research and Innovation (CM6), Rabat 10000, Morocco*
Corresponding author: ✉azarrouk@gmail.com

Received: November 13, 2023; Accepted: March 14, 2024; Published: May 14, 2024

Abstract

In this work, the effect of a new quinoxaline derivative, 2-phenyl-3-(prop-2-yn-1-yloxy) quinoxaline (PYQX), was evaluated as a corrosion inhibitor for carbon steel (CS) in 1 M HCl electrolyte. Weight loss measurement, atomic absorption spectroscopy, potentiodynamic polarization, electrochemical impedance spectroscopy, scanning electron microscopy with energy dispersive spectroscopy, and UV-vis spectroscopy were employed to assess the inhibitory activity. The electronic properties of the interaction between the inhibitor molecule and the CS substrate were studied using molecular dynamics (MD) simulation, density functional theory (DFT), and Fukui functions. According to AC impedance experiments, the inhibitor under consideration showed a maximum level of 98.1 % inhibition efficiency at 1 mM and 30 °C. The Langmuir adsorption isotherm model explains the adsorption of PYQX on the CS surface. A slope of 1 denotes a strong molecule-substrate interaction, suggesting that the binding occurs at specific surface locations. To understand

the functioning of the adsorption mechanism, various thermodynamic and activation parameters were evaluated. PDP tests demonstrated that PYQX functions as a mixed-type inhibitor. Computational correlations (DFT, MD, and Fukui indices) supported the experimental findings.

Keywords
Carbon-iron alloy; organic corrosion inhibitor; weight loss; electrochemical testing; quantum chemical calculations

Introduction

Carbon steel (CS) is often used for structural supports and components in railway systems, bridges, and other public works because of its high tensile strength, abrasion resistance, and superior surface properties [1]. However, exposure of steel to aggressive environments, such as acid-cleaning processes, can cause the metal to deteriorate and reduce its durability [2]. Corrosion inhibitors are a cost-efficient and highly effective way to mitigate the corrosive effects of steel in acidic environments [3,4].

Quinoxaline compounds have been extensively studied as corrosion inhibitors, which are environmentally safe and applicable to multiple fields such as chemistry, mechanics, and materials. It is suggested that the functional groups, conjugated multiple bonds, and aromatic rings present in quinoxaline-based molecules contribute to their excellent inhibitory performance.

Numerous corrosive conditions have been used to thoroughly assess the inhibitory abilities of these derivatives. Zarrouk *et al*. used gravimetric and electrochemical techniques to explore the impact of several quinoxaline analogs on the deterioration of copper in HNO_3 acid [5]. Recently, several authors have worked on the inhibition of corrosion of mild steel in 1 M HCl corrosive media by certain quinoxaline compounds using weight loss (WL) and electrochemical techniques, showing the high potential of quinoxaline molecules to prevent corrosion of metals [6-9]. The literature survey also showed that calculations using density functional theory (DFT) and molecular dynamic simulations (MDS) frequently provide good theoretical justifications for experimental findings in corrosion inhibition investigations [10].

In this study, the inhibitory effect of 2-phenyl-3-(prop-2-yn-1-yloxy) quinoxaline (PYQX) on CS corrosion in 1 M acidic electrolyte has been investigated. The adsorption mechanism of this quinoxaline derivative on the CS surface is further explained using quantum chemical calculations supported by DFT, Fukui functions, and molecular dynamics (MD) simulations.

Experimental

Materials and solution

In this study, CS plates with dimensions 1.5×1.5×0.3 cm were employed for testing samples. Its composition (in weight percent) is the following: C-0.3700 %, Si-0.2300 %, Mn-0.6800 %, S-0.0160 %, Cr-0.0770 %, Ti-0.0110 %, Ni-0.0590 %, Co-0.0090 %, Cu-0.1600 %, and iron (Fe) as the remaining content. The working electrode (WE) area exposed for the electrochemical corrosion test was 1 cm^2 in size. Before each use, the samples were meticulously polished with abrasive paper of increasing grain size, dried, washed with distilled water and degreased with acetone.

The electrolyte medium, 1 M HCl, was obtained by diluting concentrated 37 % analytical-grade HCl with distilled water. The synthesized compound PYQX, with the structure shown in Figure 1,

dissolves readily in 1 M HCl solution, allowing the preparation of four inhibitor assays that ranged from 10^{-3} to 1 mM.

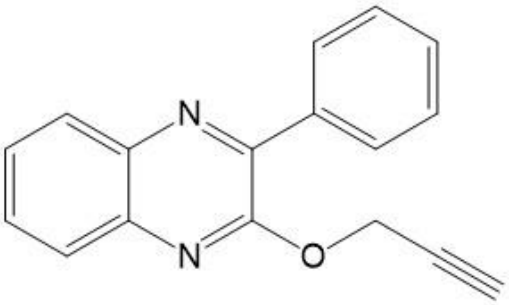

Figure 1. *Molecular structure of PYQX*

Weight loss measurements

Polished CS plates were weighed and in triplicate, placed into 50 mL glass beakers using plastic forceps. These beakers contained 1 M HCl solutions with and without various inhibitor dosages. After six hours, the samples were removed, rinsed with distilled water, dried, and re-weighed. The initial and final weights of the plates were used to determine the weight loss (WL) as Δm / mg (before and after soaking). By applying the following calculations to the weight loss data, the inhibitory effectiveness η_{WL} / % and corrosion rate (CR) (mg cm^{-2} h^{-1}) were determined by equations (1) and (2) [11]:

$$CR = \frac{\Delta m}{St} \quad (1)$$

$$\eta_{WL} = \left(1 - \frac{CR^i}{CR^u}\right) 100 \quad (2)$$

where and CR^u and CR^i are corrosion rates in the uninhibited and inhibited electrolyte.

Electrochemical testing

All electrochemical tests were carried out using a PGZ 100 potentiostat under computer control with the Voltamaster 4 program. The test model was a standard three-electrode system composed of a saturated calomel reference electrode (SCE), a platinum counter electrode, and a CS plate with an exposed surface area of 1 cm² working electrode. After observing the evolution of the open circuit potential (OCP), which usually takes approximately half an hour to stabilize, electrochemical experiments were conducted. Tafel curves were scanned by sweeping the potential with a velocity of 0.5 mV/s around the OCP in the potential range of -800 to -100 mV. The amplitude of the 10 mV peak-to-peak AC signal at OCP was used to measure the EIS at frequencies ranging from 100 kHz to 10 mHz. Impedance data were collected and presented using Nyquist and Bode plots.

The equations (3) and (4) were employed to determine the inhibition efficiency (η / %) [12]:

$$\eta_R = \left(\frac{R_p - R_p^0}{R_p}\right) 100 = 100\,\theta \quad (3)$$

where R_p and R_p^0 stand for the polarization resistance with and without inhibitor solution, respectively, while θ represents the extent of surface coverage.

$$\eta_p = \left(\frac{i_{corr}^0 - i_{corr}}{i_{corr}^0}\right) 100 \quad (4)$$

where i_{corr}^0 and i_{corr} are corrosion current densities without and with inhibitor solution, respectively.

The results for the blank obtained by two electrochemical techniques (stationary and transient) in analysing the effects of concentration and temperature were taken from the previous article [12] since the experiments were carried out under the same conditions.

Atomic absorption spectroscopy

AAS was used to quantify the metallic elements in solutions. After electrochemical tests, this method was employed to determine the iron concentration in 1 M acidic media with and without varying amounts (10^{-3} to 1 mM) of PYQX at 30 °C.

Using the atomic absorption data, the equation (5) was applied to determine the inhibition efficiency [13]:

$$\eta_A = \frac{C_{Fe}^{\ 0} - C_{Fe}}{C_{Fe}^{\ 0}} 100 \quad (5)$$

where C_{Fe}^0 and C_{Fe} represent Fe concentration in solutions without and with various PYQX amounts, respectively.

Surface characterization and electrolyte analysis

Using scanning electron microscopy with a magnification of 10000×, the surface morphologies of the CS samples were examined following their submersion in acidic media for 24 hours at 30 °C, both without and with the optimum concentration of 1 mM PYQX. At the accelerating voltage of 20 kV, energy dispersive X-ray spectroscopy (EDS) coupled with SEM was utilized to get information about the chemical composition of the material. SEM-EDS results in the absence of the inhibitor were taken from a work already published by our research team [12]. The electrolytes were carefully examined using a Jenway (series 730) UV-vis spectrophotometer before and after immersion of the CS for 72 hours at 30 °C in 1 M HCl solutions, including 1 mM of PYQX, to check for the potential formation of ferric ion-inhibitor complexes.

Computer-based research

Density functional theory (DFT) study

DFT has been utilized for a long time to assess the reactivity of organic inhibitors and correlate it to the efficiency of corrosion prevention. The program Gaussian 09 was employed to determine the DFT-based quantum physics parameters. The geometric optimization of the quinoxaline derivative PYQX in its neutral and protonated forms in the aqueous phase was produced by DFT calculations using the function B3LYP and the 6-311++G(d,p) basis set [14].

The energy gap (ΔE) energies of the lowest unoccupied molecular orbital (E_{LUMO}), highest occupied molecular orbital (E_{HOMO}), as well as the other quantum descriptors were calculated with the equations (6) to (9):

$$\Delta E = E_{LUMO} - E_{HOMO} \quad (6)$$

Global hardness (η):

$$\eta = -0.5\ \Delta E \quad (7)$$

Global electronegativity (χ):

$$\chi = 0.5\ (E_{LUMO} + E_{HOMO}) \quad (8)$$

The fraction of electrons transferred:

$$\Delta N_{110} = \frac{\chi_{Fe_{110}} - \chi_{inh}}{2(\eta_{Fe_{110}} + \eta_{inh})} = \frac{\Phi - \chi_{inh}}{2\eta_{inh}} \quad (9)$$

where Φ is the work function explains the theoretical value of χ in Fe_{110} with $\Phi = \chi(Fe_{110}) = 4.82$ eV.

Fukui indice calculations

The analysis of Fukui indices was applied to the inhibitor molecule PYQX to uncover the functional groups that enable it to interact with the iron site. This comprehensive analysis revealed that the local reactivity of PYQX was mainly attributed to the interactions between certain local reactive canters and the iron region. The dual numerical polarization basis set, consisting of the d and p orbitals, was employed in the calculations. The Fukui function is determined as the primary derivative of the electron density ($\rho(\vec{r})$) in relation to the electron number (N) in a constant external potential ($\nu(\vec{r})$) as in equation (10) [15,16]:

$$f_k = \left(\frac{\partial \rho(\vec{r})}{\partial N} \right)_{\nu(\vec{r})} \quad (10)$$

The Fukui function displays the available position in the inhibitor where nucleophilic or electrophilic assaults are most likely [15,16]. The following finite difference approximation approaches can be used to express Fukui indices for nucleophilic attack (f_k^+) and electrophilic assault (f_k^-), equations (11) and (12):

$$f_k^+ = q_k(N + 1) - q_k(N) \quad (11)$$

$$f_k^- = q_k(N) - q_k(N - 1)) \quad (12)$$

where, $q_k(N)$, $q_k(N + 1)$ and $q_k(N - 1))$ represent the neutral, cationic and anionic species, respectively.

Molecular dynamics simulations

MD was used in order to explore the interaction of the substances under study with Fe (110). Like in our previous work [16], this simulation was carried out at a similar level using the Forcite module found in the Materials Studio/8 using simulation box "2.730×2.730×3.713 nm^3" (27.30×27.30×37.13 $Å^3$). This vacuum of this box is filled by 491 H_2O, 9 H_3O^+, 9 Cl^-, and quinoxaline derivative. The Andersen thermostat was used to calibrate the system temperature to 303 K at 1000 ps simulation time and 1.0 fs utilizing the NVT ensemble, all while operating within the COMPASS force field.

Results and discussion

Weight loss and atomic absorption spectroscopy analysis

WL measurements were carried out to assess the corrosion inhibition ability of PYQX, as well as the impact of inhibitor concentration on the corrosion rate. Table 1 shows that after 6 hours of submersion, the corrosion speed of CS in the acid media was higher than that of the inhibitor solution. Simultaneously, raising the PYQX concentration from 10^{-3} to 1 mM lowered the corrosion rate from 0.321 to 0.072 mg cm^{-2} h^{-1} of CS, corresponding to an increase in inhibition effectiveness from 83.1 to 96.5 %. This demonstrates that the adsorption of inhibitor molecules protects the CS surface by blocking mass and charge transfer processes. Interestingly, the same outcomes were obtained using the atomic absorption technique (Table 1), where it was found that the addition of PYQX reduced the concentration of iron in the HCl medium. Hence, it seems that the inhibitor included in the mixture reduces steel degradation by improving the surface covering and retarding corrosion.

Table 1. *Weight loss and AAS data for CS in 1 M HCl without and with different concentrations of PYQX*

C / mM	Weight loss		Atomic absorption	
	CR, mg cm^{-2} h^{-1}	η_{WL} / %	C_{Fe} / ppm	η_A / %
0.000	1.946	-	19.286	-
0.001	0.321	83.5	3.253	83.1
0.010	0.187	90.4	2.064	89.3
0.100	0.142	92.7	1.311	93.2
1.000	0.072	96.3	0.675	96.5

Electrochemical analysis

Open circuit potential plots

Figure 2 illustrates how the open circuit potential (OCP) value changes depending on the duration of immersion of CS in 1 M HCl electrolyte medium, both with and without PYQX. It is obvious that 1800 s is long enough for the system to stabilize. It was also observed that the E_{OCP} is displaced in a positive direction following the addition of PYQX. This can result from PYQX sticking to the steel electrode surface [17]. It is noteworthy to say that there is no specific relationship between the potential shift of E_{OCP} and PYQX concentration.

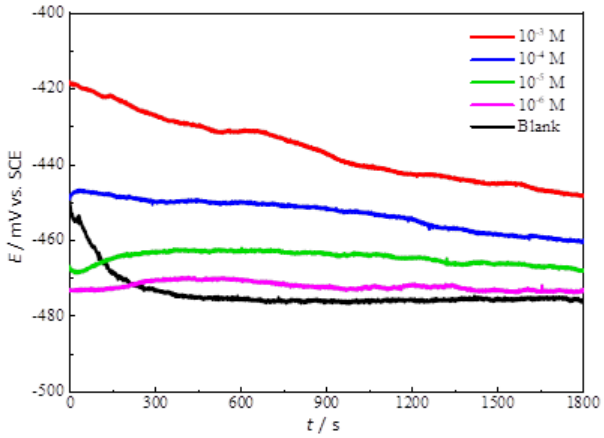

Figure 2. *Time variation in* E_{OCP} *for CS in uninhibited 1 M HCl electrolyte, and with a variety of PYQX doses*

Potentiodynamic polarization analysis

Figure 3 illustrates the PDP curves for CS performed at 30 °C in the electrolyte without and with various doses of PYQX. It is evident that including PYQX in the corrosive medium induces an overall reduction in cathodic and anodic current densities, which becomes more pronounced with increasing amounts of PYQX. This result suggests that PYQX reduces anodic oxidation and retards the reduction of H^+ protons [17]. The reduction trend of the cathodic segment was greater than that of the anodic segment, suggesting that PYQX has a greater protective influence on the cathodic reaction than on the anodic reaction. On the downside, the cathodic portions are linear, indicating that PYQX has little influence on the H^+ ion reduction mechanism and that the H^+ reduction reaction at the CS interface occurs mainly by a pure activation [17].

Table 2 presents the outcomes of inhibition effectiveness (η_P / %), as well as electrochemical corrosion factors such as corrosion current density ($i_{corr.}$), corrosion potential (E_{corr}), and Tafel slopes (cathodic (β_c) and anodic (β_a)) for different concentrations of PYQX, obtained by extrapolation of the linear cross-sections of the anodic and cathodic polarization plots at E_{corr} [18]. Analysing the corrosion potential allows the inspection of the inhibition mechanism of inhibitor molecules. The shift in E_{corr} with PYQX injection was significantly less than 85 mV from baseline, a value considered a threshold

for identifying the type of inhibitor. The slight shift in E_{corr} following the addition of the inhibitor demonstrated that investigated molecules function as a mixed-type inhibitor by limiting CS oxidation and H^+ ion reduction. It follows that surface adsorption, leading to the formation of a coating layer covering the active sites, is the primary mechanism behind the inhibitory activity of PYQX [18]. The η_P increases as the inhibitor PYQX concentration increases, peaking at 98.1 % at 1 mM. This result agrees well with the conclusions of the measures of atomic absorption and weight loss.

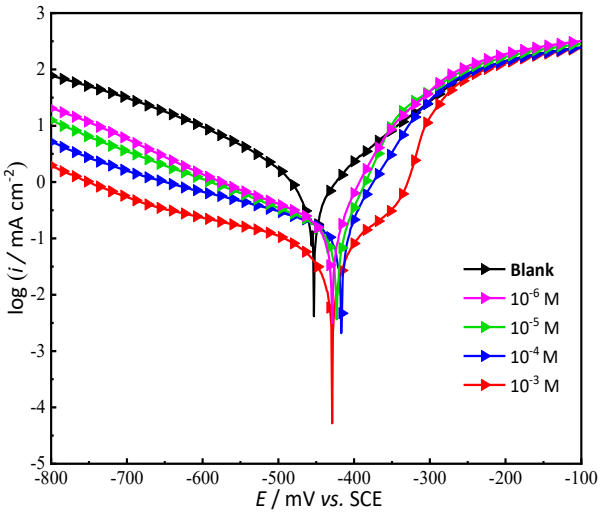

Figure 3. *PDP curves for CS in uninhibited 1 M HCl electrolyte and with a variety of PYQX doses*

Table 2. *PDP factors and η_P for CS corrosion in the uninhibited 1 M HCl electrolyte and with a variety of PYQX doses*

C/ mM	-E_{corr}/ mV *vs*. SCE	-β_c /mV dec^{-1}	β_a / mV dec^{-1}	i_{corr} /µA cm^{-2}	η_P / %
0.000	456.3	155.4	112.8	1104.1	----
0.001	432.2	119.9	71.9	107.6	90.3
0.010	426.1	122.3	85.5	91.2	91.7
0.100	420.3	87.6	62.6	51.2	95.4
1.000	432.1	114.1	75.5	21.3	98.1

Electrochemical impedance spectroscopy analysis

Electrochemical impedance spectroscopy (EIS) is generally used to explore the mechanisms of charge transfer, surface passivation, and corrosion inhibition at the metal-electrolyte interface. Typically, Nyquist and Bode curves are employed to highlight these outcomes of EIS. The properties of corrosion prevention of quinoxaline derivative on CS have already been explored by EIS [19]. Nyquist impedance plots and Bode impedance modulus and phase angle plots of CS in the uninhibited electrolyte and with a variety of PYQX doses at 30 °C are shown in Figures 4 and 5, respectively.

Nyquist plots (Z_i *vs*. Z_r) presented in Figure 4 show that just one capacitive loop has an identical form for all experienced inhibitor concentrations. These similar impedance responses indicate that the presence of PYQX did not alter the corrosion mechanism significantly, and the charge transfer is the primary factor controlling the process of corrosion. Similarly, Figure 4 reveals that the capacitive loop diameter rises with a rising dose, thus indicating inhibition efficiency. The obvious rise of impedance modulus $|Z|$ at low frequencies, as evident in the Bode graphs (Figure 5), implies the rise of charge transfer resistance with the rise of the inhibitor concentration. This could be a confirmation of better coverage with the increase of PYQX dose, related to the planar geometry of the quinoxaline derivative, which may boost the adsorption of this substance on the CS surface by creating a barrier coat that prevents corrosion [19]. The phase angle diagrams present only one

peak, revealing that the corrosion process requires only one stage and is governed by charge transfer. With increasing inhibitor concentration, the phase angles at corresponding peaks attained higher negative values due to considerable molecular adsorption, suggesting that the tested inhibitor PYQX may be involved in creating a protective layer on the metal substrate [20-22].

The experimental Nyquist and Bode diagrams for PYQX were adjusted using the equivalent electrical circuit depicted in Figure 6. The equivalent circuit in Figure 6 includes a solution resistance (R_s), a polarization resistance (R_p), and a constant phase element (CPE) describing a contribution of double-layer impedance. Equation (13) can be utilized to determine the expression for the impedance of the CPE [19]:

$$Z_{CPE} = \left[\frac{1}{Q(i\omega)^n} \right] \tag{13}$$

where Q, i, ω and n are CPE constant, imaginary number, angular frequency ($\omega = 2\pi f$, where f is frequency), and CPE exponent, which can be used to measure the roughness or heterogeneity of the surface, respectively.

The double layer capacity (C_{dl}) of an adsorbed film is connected to the CPE settings in accordance with equation (14):

$$C_{dl} = \left[QR_p^{1-n} \right]^{1/n} \tag{14}$$

The impedance parameter values retrieved and determined by fitting EEC in Figure 6 to EIS results in Figures 4 and 5 are presented in Table 3, together with calculated values for inhibitor efficacy using eq. (4), and chi-square (χ^2) values obtained after impedance data fitting procedure. Low values of χ^2 indicate a strong correlation between impedance data obtained by the chosen model and the measured outcomes. This suggests that there is a good concordance between the two sets of data.

Data in Table 3 generally show that the value of R_p rises as PYQX content does. This rise leads to the protection of the CS and reduces the number of active sites produced by binding the negatively charged Cl^- ions to the surface of CS. The simultaneous reduction in C_{dl} values can be ascribed to a decline in the local dielectric constant and/or an augmentation in the thickness of the electrical double layer, indicating the adsorption of the studied molecules onto the metal surface [12].

The EIS study gave an inhibitory efficiency of about 97.1 % for a concentration of 1.0 mM PYQX at 30 °C. This confirms the previous results obtained by WL, AAS and PDP.

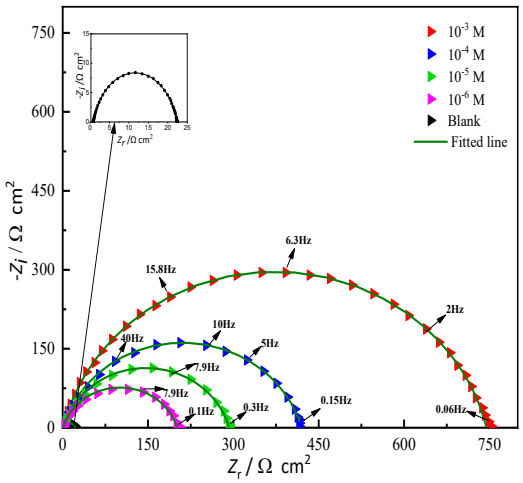

Figure 4. *Nyquist impedance curves for CS in uninhibited 1 M HCl electrolyte and with a variety of PYQX doses*

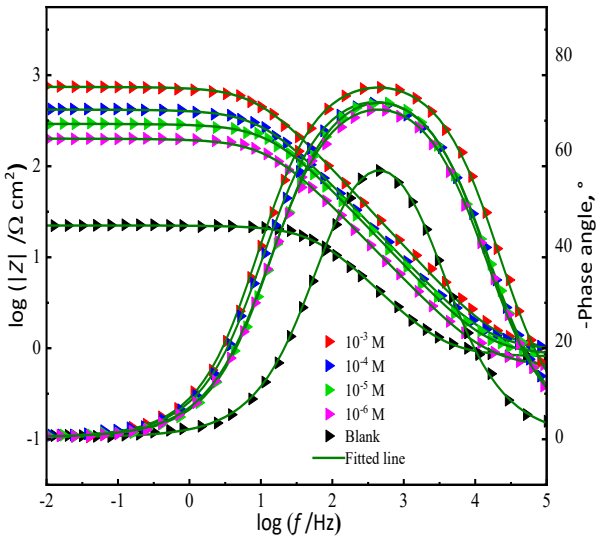

Figure 5. *Bode graphs for CS in uninhibited 1 M HCl electrolyte and with a variety of PYQX doses*

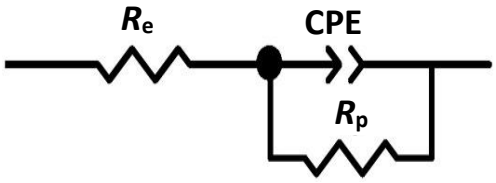

Figure 6. *The electrical equivalent circuit model*

Table 3. *EIS variables and inhibitory effectiveness for CS in the uninhibited 1M HCl electrolyte and with a variety of PYQX doses*

C / mM	R_s/Ω cm^2	R_p/Ω cm^2	Q / 10^{-6} Ω^{-1} s^n cm^{-2}	n	C_{dl} / μF cm^{-2}	χ^2	η_R / %	θ
0.000	0.83	21.57	293.9	0.845	116.2	0.002	---	---
0.001	0.80	200.5	78.0	0.847	36.8	0.004	89.2	0.892
0.010	0.86	291.5	64.1	0.850	31.8	0.003	92.6	0.926
0.100	1.01	418.6	49.3	0.854	25.4	0.006	94.8	0.948
1.000	0.96	743.8	35.5	0.866	20.2	0.009	97.1	0.971

Adsorption isotherm

After adhering to the metal/solution contact, organic molecules restrict the dissolution of C▪S. Thus, it is needed to investigate the adhesion property of PYQX molecules on the C▪S contact. To achieve this goal, a variety of adsorption models were investigated in the present research., including the Langmuir, Freundlich, El-Awady, Temkin, and Flory-Huggins isotherms. Finally, the results of this study indicate that the Langmuir model is the best-suited model for characterizing the adsorption of PYQX onto the CS contact, which can be expressed by equation (15):

$$\frac{\theta}{1-\theta} = K_{ads} C_{inh} \quad (15)$$

where C_{inh}, K_{ads}, and θ are the PYQX concentration, the equilibrium adsorption constant and the extent of surface coverage, respectively.

The standard Gibbs free energy of adsorption ΔG_{ads}^0 is related to the K_{ads} according to equation (16) [20]:

$$\Delta G_{ads}^0 = -RT \ln(55\, K_{ads}) \quad (16)$$

where 55.5 is the concentration of water in solution, R and T are gas constant and absolute temperature (303 K), respectively.

The Langmuir isotherm graph is illustrated in Figure 7. It has already been recognised that when ΔG_{ads}^0 > -20 kJ mol^{-1}, inhibitor molecules are adsorbed onto the CS surface by electrostatic interactions (physisorption), while when ΔG_{ads}^0 < -40 kJ mol^{-1}, inhibitor adsorption occurs through the formation of coordination bonds (chemisorption) between compound molecules and the CS surface. In cases where -40 kJ mol^{-1} < ΔG_{ads}^0 < -20 kJ mol^{-1}, inhibitor adsorption occurs through both physisorption and chemisorption [20].

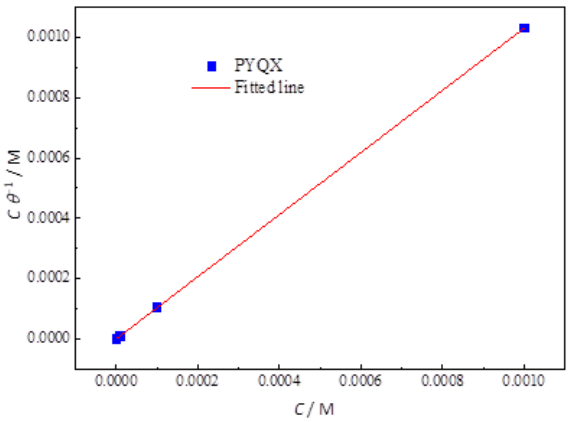

Figure 7. *Langmuir isotherm graph for PYQX adsorption on the CS in 1 M HCl at 30 °C*

R^2 value of linear regression in Figure 7 is 1, indicating a close-to-perfect linear correlation. This affirms that the Langmuir adsorption model applies to the adsorption process of PYQX in the corrosion test. This data suggests that the adsorption process between PYQX and the corrosion system is highly efficient, allowing for consistent and reliable results. The negative value of ΔG_{ads}^0 and the high value of K, which takes on the value 988660.069 L mol^{-1}, demonstrate the durability of the bilayer taken up on the CS interface, resulting in a higher effectiveness of inhibition [21]. Additionally, the calculated value of ΔG_{ads} in this study is equal to -44.89 kJ mol^{-1}, which reveals that adsorption of 2-phenyl-3-(prop-2-yn-1-yloxy) quinoxaline on the CS surface is mainly through chemisorption.

Temperature effect

In pickling, inhibitors are employed to guard against an acidic assault on metal equipment. Pickling processes are often carried out at high temperatures. For application, a corrosion inhibitor must maintain its effectiveness in a corrosive system at specific working temperatures. The research has clearly established that when temperature increases, organic molecules are desorbed from surfaces, which then results in increased corrosion of metals. This phenomenon has been documented and observed in numerous studies. Therefore, it is doubtful that higher temperatures can cause enhanced metal corrosion [21].

In the interest of investigating how temperature affects the efficiency of PYQX, PDP tests were carried out in the uninhibited electrolyte and with 1 mM PYQX at temperatures fluctuating between 30 to 60 °C (Figure 8). The inhibitor efficiency values (η) and electrochemical variables calculated for this study are presented in Table 4. The results show that an elevation in temperature produces higher i_{corr} values and this effect is greater in the uninhibited electrolyte. This means that the rise in temperature speeds up the disintegration of the CS by causing desorption of the PYQX molecules from the CS surface.

The η_p dropped from 98.1 to 91.6 %, demonstrating that PYQX underwent desorption from the CS surface, and consequently, the degree of surface coverage decreases as the adsorption-desorption equilibrium shifts in favour of inhibitory desorption [21].

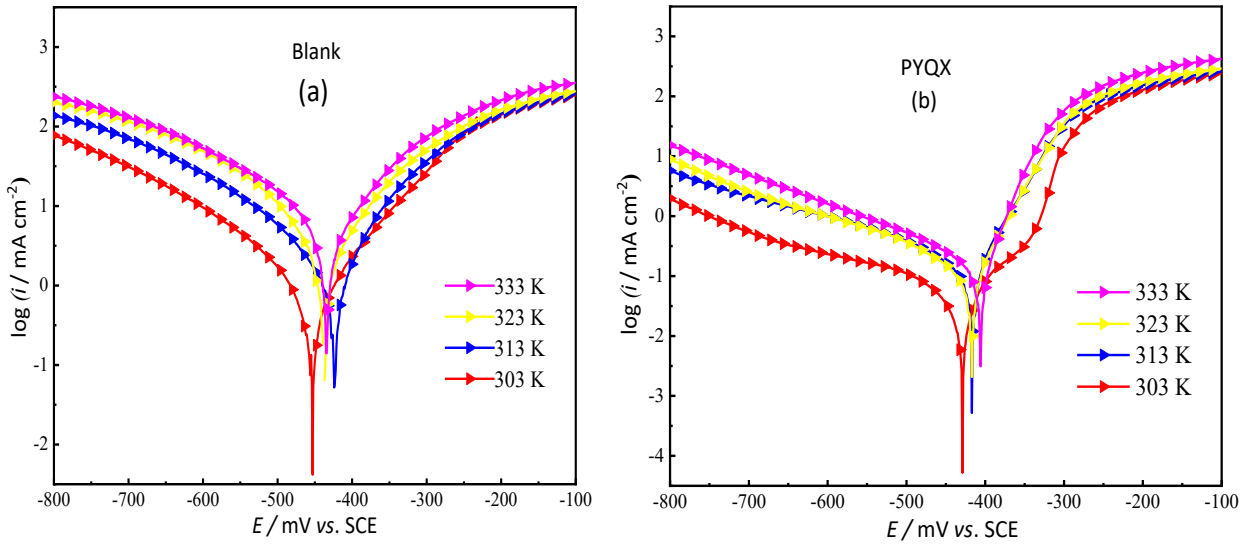

Figure 8. *PDP graphs of CS in 1 M HCl electrolyte (a) - without and (b) - with 1.0 mM of PYQX, at different temperatures*

Table 4. *PDP electrochemical variables of CS in 1 M HCl electrolyte without and with 1 mM of PYQX, at different temperatures*

Medium	T / K	$-E_{corr}$ / mV *vs.* SCE	$-\beta_c$ / mV dec^{-1}	β_a / mV dec^{-1}	i_{corr} / µA cm^{-2}	η_p / %
Blank electrolyte	303	456.3	155.4	112.8	1104.1	-----
	313	423.5	131.3	91.3	1477.4	----
	323	436.3	117.8	91.4	2254.0	-----
	333	433.3	134.6	103.9	3944.9	-----
PYQX	303	432.1	114.1	75.5	21.3	98.1
	313	420.0	109.5	62.0	79.3	94.6
	323	420.5	127.0	71.5	138.4	93.9
	333	409.3	174.2	52.5	329.5	91.6

Activation parameters

The descriptors of the important indices, which are activation energy (E_a), enthalpy change (ΔH_a), and entropy change (ΔS_a), were determined in order to better understand how temperature affects the inhibition mechanism. The E_a value of the corrosion process at varying temperatures, both without and with 1 mM of PYQX was computed by applying the Arrhenius equation (17) [22]:

$$i_{corr} = A e^{\frac{-E_a}{RT}} \quad (17)$$

ΔH_a and ΔS_a were computed by using the following alternative Arrhenius equation (18) [22]:

$$i_{corr} = \frac{RT}{Nh} e^{\frac{\Delta S_a}{R}} e^{-\frac{\Delta H_a}{RT}} \quad (18)$$

where A, R, T, N, and h are the pre-exponential constant, gas constant, absolute temperature, Avogadro number, and Planck's constant, respectively.

The E_a value for CS oxidation was calculated without and with 1.0 mM of PYQX using the slope ($-E_a/R$) of the plot presented in Figure 9, which shows the dependency of ln(i_{corr}) on 1/T. Likewise, by

tracing ln(i_{corr}/T) as a function of 1/T under the same conditions (Figure 10), the slope calculates the values of ΔH_a, while the y-intercept calculates the values of ΔS_a. The activation energy and thermodynamic parameters resulting from the Arrhenius and the transition state plots are reported in Table 5.

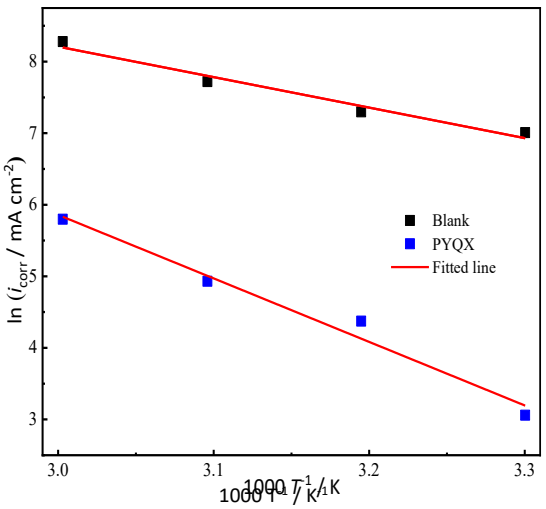

Figure 9. *Arrhenius plots for CS in uninhibited 1 M HCl electrolyte and with 1 mM of PYQX*

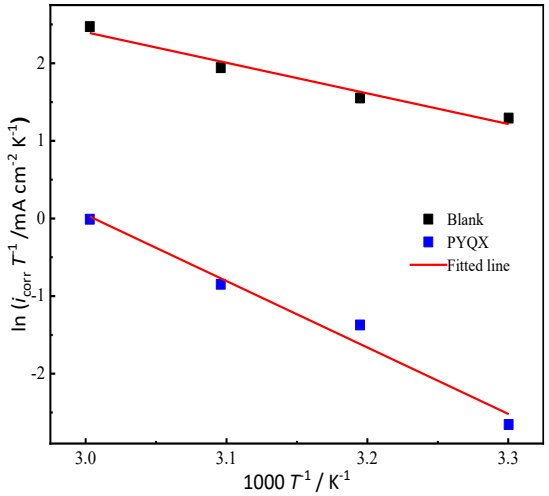

Figure 10. *Transition-state plots for CS in uninhibited 1 M HCl electrolyte and with 1 mM of PYQX*

It has been noted in Table 5, that when 10^{-3} M of PYQX is present, the E_a value is greater than that of the uninhibited electrolyte, suggesting that there is an energy barrier between the CS surface and inhibitor molecules under study. The oxidation process of the CS substrate is endothermic, as indicated by the positive sign of the activation enthalpy change (ΔH_a). In addition, the existence of PYQX increased the value of ΔH_a, stating that the dissolution of CS is difficult due to the adsorption of PYQX molecules on the CS surface. On the other side, ΔS_a value attains a high positive value compared to the uninhibited medium, indicating an increase in disorder of the system occurs throughout the adsorption process of the transformation from reactant molecules to activated complexes [23].

Table 5. *Activation energy and thermodynamic parameters of CS in uninhibited 1 M HCl electrolyte and with 1 mM of PYQX*

Medium	E_a /kJ mol^{-1}	ΔH_a/ kJ mol^{-1}	ΔS_a /J mol^{-1} K^{-1}
Blank electrolyte	35.4	32.8	-79.2
PYQX	73.8	71.2	16.3

Scanning electron microscopy and energy-dispersive X-ray spectroscopy analysis

Surface examination by scanning electron microscopy (SEM) scanning technique was completed to generate evidence of the impact of inhibitor compounds on the microstructure of the CS surface and to confirm the creation of a protected layer by PYQX on the substrate. Figure 11 displays CS surface SEM micrographs after 24 h of soaking in the uninhibited medium [23] and with 1 mM of PYQX.

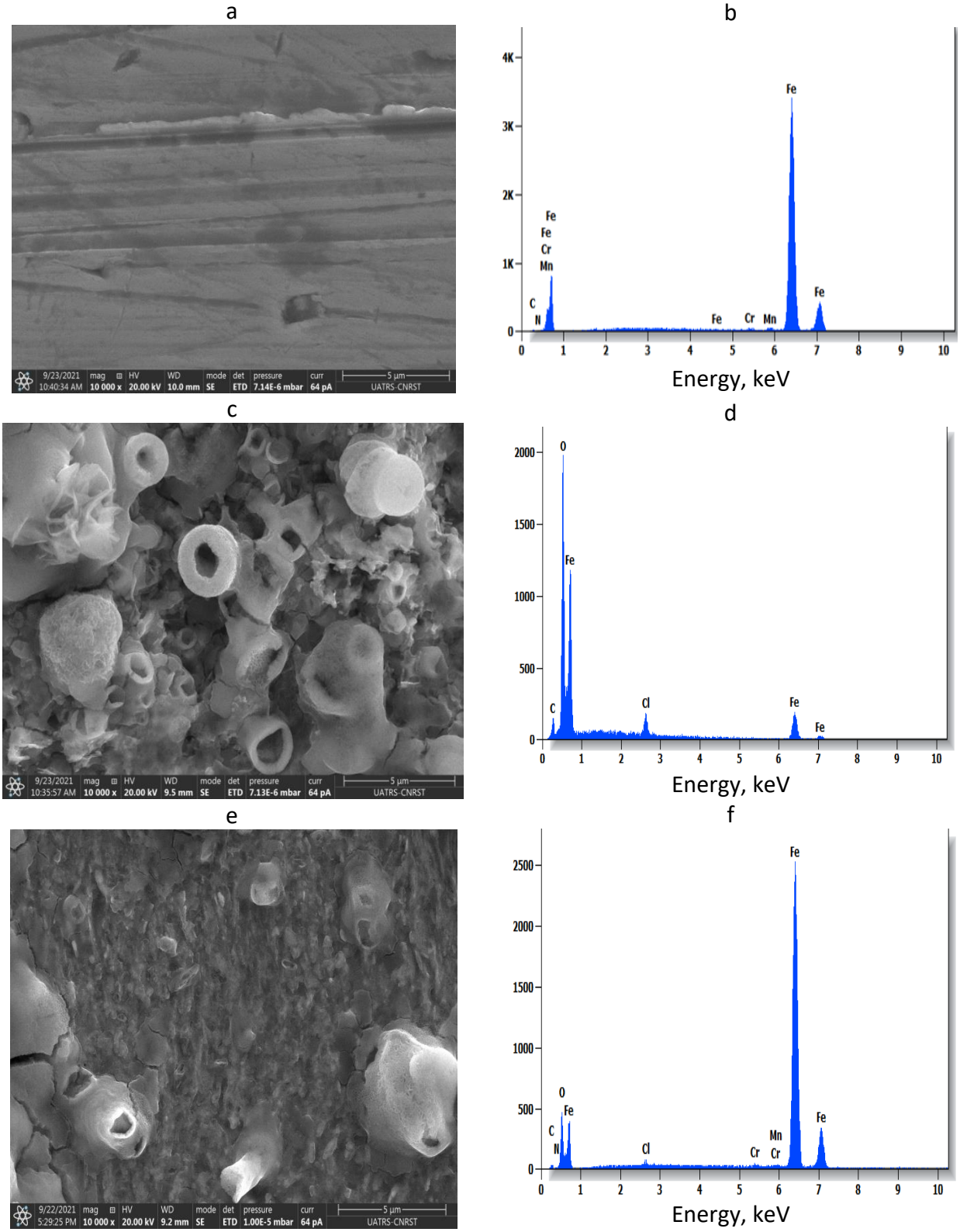

Figure 11. *SEM/EDS photographs obtained: immediately after polishing (a/b), 24 hours after soaking in 1 M HCl media (c/d), and 24 hours after soaking in 1 M HCl media with 1 mM PYQX (e/f). SEM images (a) and (c) are taken from [12]*

Figure 11(a) shows that the polished CS surface has many scratches from polishing. It is clear from Figure 11(c) that the morphology of the entire CS area after immersion in the uninhibited medium is severely damaged, while Figure 11(e) shows that the surface morphology greatly improves when 1 mM PYQX is present in the solution. This shows that the inclusion of PYQX leads to a reduction in the number of active corrosion centres by adsorption of the molecules of PYQX on the surface of the CS substrate, thus creating a stable, protective film. The EDS spectrum for the polished CS presented in Figure 11(b) showed a strong iron peak and peaks characteristic for the chemical composition of the CS sample. After immersion of the CS in the HCl electrolyte, the EDS spectrum in Figure 11(d) shows strong Cl and O peaks, suggesting the existence of oxides and chlorides in the corrosion products. On the surface of the specimens exposed to the PYQX-inhibited acidic electrolyte, a remarkable reduction in Cl content is revealed in Figure 11(f), which confirms the adsorption of PYQX molecules on the area of CS.

UV– visible spectra analysis

UV-visible spectrometry was applied to see how CS and molecules of PYQX interact. The absorption spectra of corrosive media, including 1 mM of PYQX, before and after 72 h of CS soaking, are plotted in Figure 12. As in previous research [24], a change in the location of the absorbance peak or a change in the amplitude of the absorbance indicates the development of a complex between two species present in the acidic electrolyte. A careful examination of the absorption spectra showed a notable shift in the absorption bands from 252 to 254 nm and 321 to 327 nm. Furthermore, a remarkable increase in the absorption maximum (λ_{max}) and the appearance of an additional peak at 226 nm reflects the interaction between the studied PYQX compounds and Fe^{2+} ions in the solution. These findings demonstrate the development of a complex between quinoxaline molecules and Fe^{2+} ions in the acidic media [25].

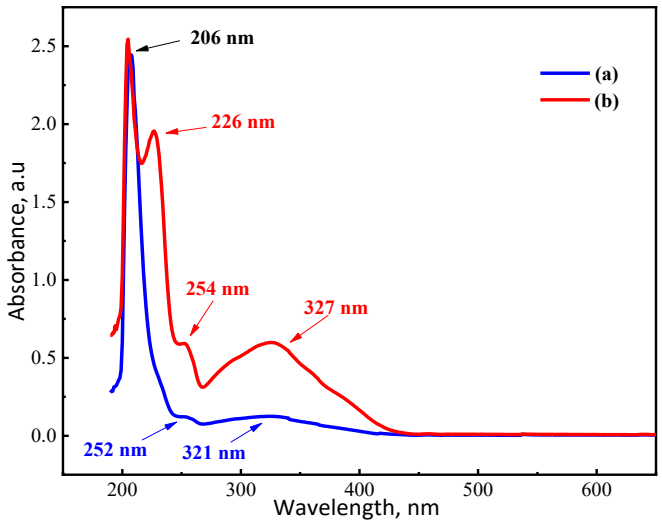

Figure 12. *UV-visible spectra of 1 M HCl including 1 mM of PYQX (a) -before and (b) - after 72 hours of CS immersion*

Density functional theory reactivity

A molecule with heteroatoms in its structure binds one or more H^+ protons in an acidic medium, which can modify its chemical reactivity. Figure 13 shows the percentage distribution of the different protonated forms *vs.* pH using MarvinView software, suggesting that in dependence on pH, the PYQX molecule likely protonates in two forms.

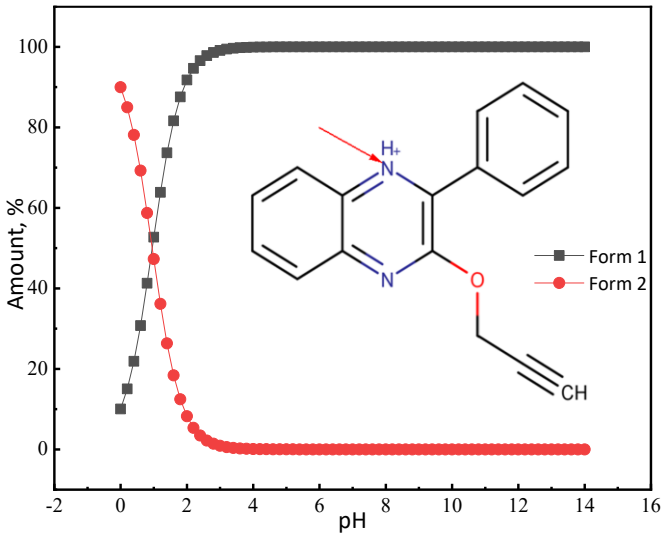

Figure 13. *Content of different protonated forms of PYOX as a function of pH*

The optimal protonation occurs at position 2, wherein the nitrogen atom (sp^2-hybridized) within the foundational structure of quinoxaline is in closer proximity to the protons of the benzene ring, thereby inducing a change in the neutral state of PYQX. Therefore, the current analysis is intended to follow the reactivity behaviour of two forms, neutral and protonated.

To investigate the effectiveness of corrosion inhibition and evoke a plausible corrosion inhibition mechanism, the electronic properties, global activity descriptors and local activity indices of PYQX neutral and charged were calculated [26]. To maintain structural conformity, the absence of imaginary frequencies must be ascertained using the same level of theory. To plot the structure, HOMO and LUMO of the compounds, GaussView/5 software [27] was applied.

Figure 14 depicts the energy-minimized structures and FMOs (HOMO and LUMO) of the PYQX neutral and charged. For the two forms in question, it is noticeable that the distribution of FMOs is total over the structure of both forms of the PYQX, implying that the reactivity is very high with other species and especially with the metal surface.

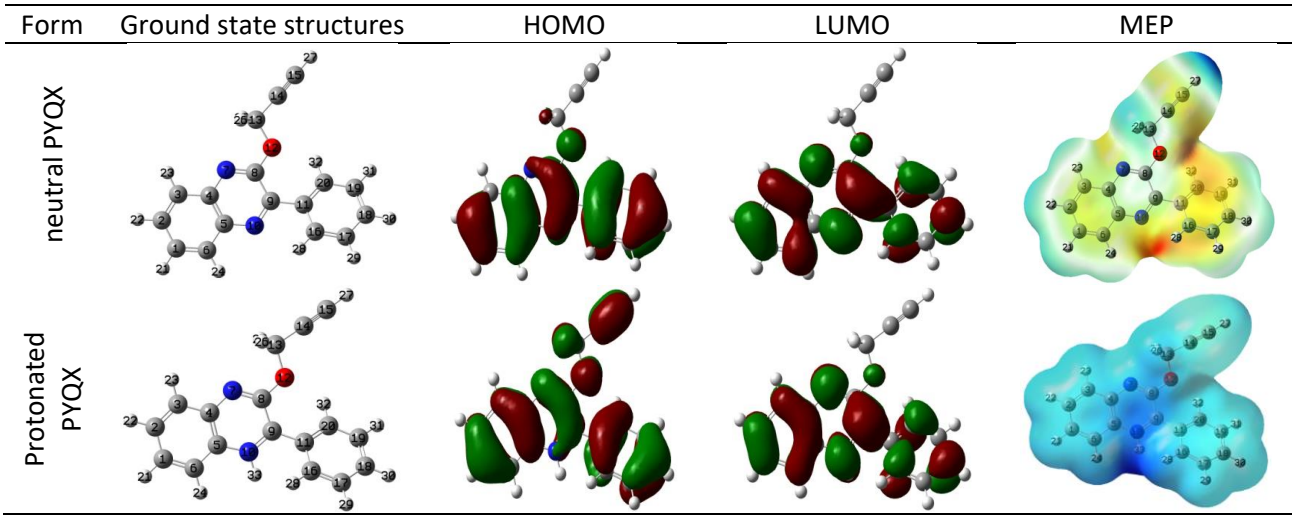

Figure 14. *Optimized state structure (FMO), and molecular electrostatic potential (MEP) of the neutral and charged PYQX*

E_{HOMO} and E_{LUMO} values serve to assess the donor/acceptor ratio in the molecule/metal relationship [26]. In this study, the reactivity of the PYQX neutral and charged is followed by these two descriptors. Table 6 groups different values of the reactivity descriptors of both forms. It is

revealed in Table 6 that the PYQX neutral is more nucleophilic (E_{HOMO}=-6.103 eV) and the PYQX charged is more electrophilic (E_{LUMO}=-6.835 eV). Therefore, ΔE (E_{LUMO}-E_{HOMO}) allows to measure the reactivity of a molecule, as the most minimal value of this descriptor means that the specific reactivity is maximal [26]. The description comparison between the values for both forms of this descriptor (ΔE) shows that the charged PYQX is more reactive with a low value of 3.453 eV.

The electronegativity (χ) presents an attractive power of the electrons of a chemical species; the relevance of the descriptor translates the reactivity of interaction [26]. The value of 8.561 eV for the charged PYQX, as shown in Table 6, indicates that it is a more reactive inhibitor on surfaces with a negative charge. The reactivity and hardness (η) of a molecule are reciprocally proportional: a harder molecule implies lower reactivity [26]. The data in Table 6 show that charged PYQX (1.726 eV) is more reactive. The fraction of electron transferred (ΔN_{110}) values provide useful information on the tendency of electrons to flow from the inhibitor molecule to the CS surface ($\Delta N > 0$), or from the carbon steel to the inhibitor ($\Delta N < 0$) [28]. In this present computation, the neutral PYQX molecule (ΔN_{110} = 0.197) is more likely to share its electrons in order to form coordination bonds with Fe (110).

Table 6. *Chemical descriptors of neutral and charged PYQX molecules*

Form	E_{HOMO} / eV	E_{LUMO} / eV	ΔE / eV	χ / eV	η / eV	ΔN_{110}
PYQX neutral	-6.103	-1.865	4.238	3.984	2.119	0.197
PYQX protonated	-10.288	-6.835	3.453	8.561	1.726	-1.084

The inhibitory efficacy of a molecule can be measured and assessed by the prevalence of active sites throughout its structure. In addition, the sites of high local reactivity support substantial inhibitory efficacy. These centres may bind with others located at the metal surface by chemical bonds [29]. In Table 7, the various sites of PYQX molecule neutral and charged are collected, respectively, with the most suitable atoms presenting the highest reactivity, giving the acceptor (nucleophilic attack (f^+)) and donor (electrophilic- attack (f^-)).

Table 7. *Atoms of local reactivity for neutral and charged PYQX molecule*

Atom	PYQX molecule neutral		PYQX molecule charged	
	f^-	f^+	f^-	f^+
C (1)	0.034	0.052	0.019	0.047
C (2)	0.062	0.054	0.030	0.057
C (3)	0.056	0.050	0.023	0.037
C (4)	0.024	0.038	0.016	0.045
C (5)	0.034	0.038	0.019	0.047
C (6)	0.063	0.051	0.027	0.042
N (7)	0.040	0.107	0.017	0.078
C (8)	0.023	0.056	0.016	0.087
C (9)	0.035	0.065	0.015	0.047
N (10)	0.057	0.106	0.032	0.107
C (11)	0.055	0.012	0.054	0.008
O (12)	0.015	0.025	0.016	0.037
C (13)	0.007	0.007	0.023	0.010
C (14)	0.011	0.004	0.109	0.010
C (15)	0.030	0.022	0.148	0.032
C (16)	0.048	0.030	0.041	0.021
C (17)	0.039	0.022	0.038	0.019
C (18)	0.074	0.036	0.069	0.028
C (19)	0.041	0.020	0.039	0.017
C (20)	0.034	0.023	0.022	0.016

The condensed Fukui functions (f^+ and f^-) for PYQX neutral indicated that C2, C3, C6, N10, C11, C16, and C18 are the most electrophilic attacks centres, whereas the C1, C2, C3, C6, N7, C8, C9, and N10 are highest nucleophilic attacks centres. These sites are suitable for donating and accepting electrons. After protonation, the electron-donating effect decreased noticeably while the electron-attracting effect increased.

Molecular dynamics simulation

Molecular dynamics (MD) simulation is a valuable approach to describe better and understand the adsorption pattern of a molecular substance on a metallic material [30]. In this work, the simulation deals with the reactivity of quinoxaline molecules (neutral and charged) and Fe (110). This research also investigated the reactivity model of two molecule forms on the effectiveness of surface protection against attack by corrosive species contained in the molar HCl solution. Figure 15 illustrates the adsorption of the species of interest (lateral and top representations) onto Fe (110). Further analysis of these two configurations reveals that both molecules adsorb wholly and largely occupy the iron atomic layer, resulting in a high content of anticorrosive protection.

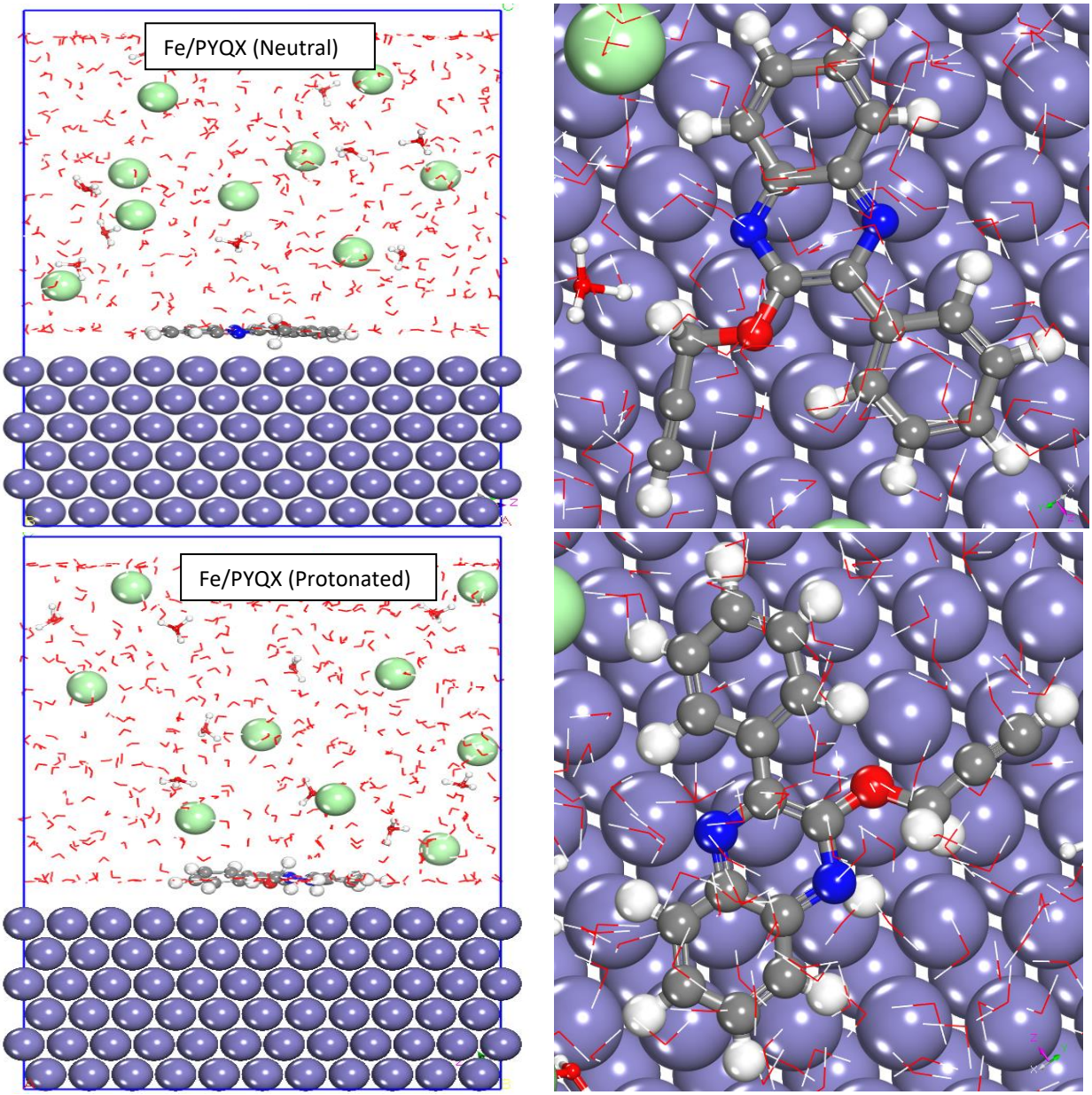

Figure 15. *Adsorption configurations of neutral and charged PYQX molecule onto Fe (110)*

The interaction energy (E_{inter}) value is established by the equation (19) [31]:

$$E_{inter} = - E_{(surface+ solution)} - E_{inhibitor} + E_{total} \quad (19)$$

The E_{inter} with a low value indicates the big interactions for both systems Fe/ PYQX (neutral) and Fe/PYQX (charged). It appears from the comparative study that the most negative value of Fe/PYQX (charged) with -889.929 kJ mol^{-1} reflects a big interaction. These simulation data clearly prove the agreement compared with the quantum computations.

The primary objective of this model is to assess the significance of adsorption by utilizing inter-atomic distances for Fe/PYQX (neutral), which is equal to -888.428 kJ mol^{-1}, and Fe/PYQX (charged), which is equal to -889.929 kJ mol^{-1}, through the introduction of the radial distribution function (RDF). The published literature confirms that the likelihood of chemical adsorption is higher when the bond length is less than 0.35 nm (3.5 Å). By contrast, physical adsorption is more probable [31]. In Figure 16, the 1st peak displays the bond lengths for both systems are less than 0.35 nm.

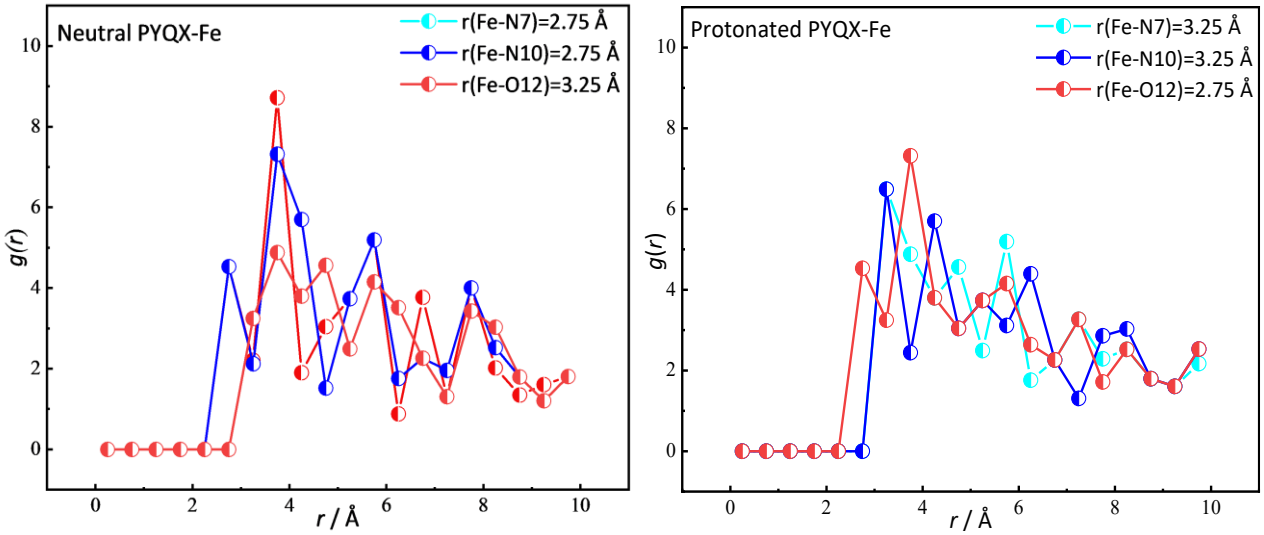

Figure 16. *RDF (g(r)) of Fe/ PYQX (neutral) and Fe/PYQX (charged) (1 Å = 0.1 nm)*

Inhibitory mechanism

The adsorption process of inhibitor on a metal surface explains the mechanism of corrosion inhibition. Figure 17 shows a possible mechanism for the adsorption of PYQX on the C▪S surface in 1 M HCl. Organic molecules adsorb on metal surfaces primarily by chemisorption, physisorption, or both. In this study, PYQX has many functional groups, such as O and N heteroatoms and heterocycles, that can help the inhibitor stick to the surface. Organic compounds present both neutral and protonated forms when their heteroatoms undergo protonation in acidic environments. A positive charge may form on the metal surface as a result of fast metal oxidation. A negatively charged surface may emerge as a result of the positive charge attracting chloride ions present in the solution.

The protonated form then physically adheres to the newly formed negatively charged surface. This creates a protective layer that slows down the anodic corrosion process. Also, the positively charged ions that stick to the cathodic sites compete with H^+ for electrons, which lowers the production of H_2 [32]. The neutral form of PYQX chemisorbed to the metal surface through interactions between the empty d-orbital of Fe atoms and the free electron pairs of heteroatoms (N, O). The transfer of excess negative charge from the Fe d-orbital to the unoccupied π* orbital of inhibitor molecules can occur on the CS surface, leading to greater inhibitor adsorption on the steel surface. Moreover, between the aromatic cycles and the d-orbitals of the CS surface, electron retro-donation

may occur [33]. At last, a barrier is created on the steel surface by an adsorbed inhibitor film to prevent metal corrosion from the corrosive medium.

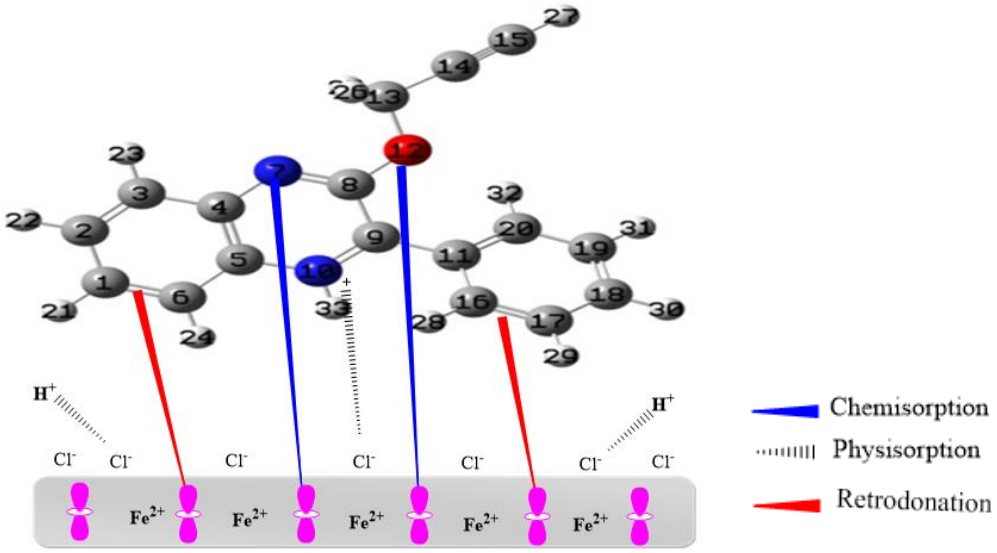

Figure 17. *Schematic illustrating of PYQX adsorption mechanism on the C-S surface in chloride solution*

Conclusion

Corrosion inhibition of carbon steel was investigated in a molar hydrochloric acid environment using a novel quinoxaline derivative. The study used a combination of chemical and electrochemical techniques, as well as some theoretical simulations. The main results of this research can be resumed as follows:

PYQX demonstrated exceptional inhibitory efficacy against CS corrosion in acidic electrolytes. As the concentration increases, its performance strengthens, reaching 98.1 % at 1 mM.

- PYQX is a mixed-type inhibitor with a cathodic inclination, as indicated by the PDP profiles, which show that it significantly inhibits cathodic hydrogen evolution processes and anodic metal dissolution. EIS analyses showed that when PYQX is present, R_p values go up and double-layer capacitance decreases. This shows that the inhibitor can slow down CS corrosion.
- The chemisorption mechanism of PYQX adsorption on the CS interface is consistent with the Langmuir adsorption isotherm.
- Surface and electrolyte investigations (SEM, EDS, and UV-visible) showed that a protective coating has formed over the surface of CS.
- DFT and MD simulations showed high reactivity with CS (Fe (110)).

References

[1] M. M. Shaban, N. A. Negm, R. K. Farag, A. A. Fadda, A. E. Gomaa, A. A. Farag, M. A. Migahed, Anti-corrosion, antiscalant and anti-microbial performance of some synthesized trimeric cationic imidazolium salts in oilfield applications, *Journal of Molecular Liquids* **351** (2022) 118610. https://doi.org/10.1016/j.molliq.2022.118610

[2] H. E. Hashem, A. A. Farag, E. A. Mohamed, E. M. Azmy, Experimental and theoretical assessment of benzopyran compounds as inhibitors to steel corrosion in aggressive acid solution, *Journal of Molecular Structure* **1249** (2022) 131641. https://doi.org/10.1016/j.molstruc.2021.131641

[3] S. M. Shaban, E. Badr, M. A. Shenashen, A. A. Farag, Fabrication and characterization of encapsulated Gemini cationic surfactant as anticorrosion material for carbon steel

protection in down-hole pipelines, *Environmental Technology and Innovation* **23** (2021) 101603. https://doi.org/10.1016/j.eti.2021.101603

[4] E. A. Mohamed, H. E. Hashem, E. M. Azmy, N. A. Negm, A. A. Farag, Synthesis, structural analysis, and inhibition approach of novel eco-friendly chalcone derivatives on API X65 steel corrosion in acidic media assessment with DFT & MD studies, *Environmental Technology and Innovation* **24** (2021) 101966. https://doi.org/10.1016/j.eti.2021.101966

[5] A. Zarrouk, A. Dafali, B. Hammouti, H. Zarrok, S. Boukhris, M. Zertoubi, Synthesis, characterization and comparative study of functionalized quinoxaline derivatives towards corrosion of copper in nitric acid medium, *International Journal of Electrochemical Science* 5 (2010) 46–55. https://doi.org/10.1016/S1452-3981(23)15266-7

[6] F. Benhiba, R. Hsissou, Z. Benzekri, S. Echihi, J. El-blilak, S. Boukhris, A. Bellaouchou, DFT / electronic scale, MD simulation and evaluation of 6-methyl-2- (p-tolyl) -1 , 4-dihydroquinoxaline as a potential corrosion inhibition, *Journal of Molecular Liquids* **335** (2021) 116539. https://doi.org/10.1016/j.molliq.2021.116539

[7] M. Ouakki, M. Galai, Z. Benzekri, C. Verma, E. Ech-chihbi, S. Kaya, S. Boukhris, E. E. Ebenso, M. E. Touhami, M. Cherkaoui, Insights into corrosion inhibition mechanism of mild steel in 1 M HCl solution by quinoxaline derivatives : electrochemical, SEM/EDAX, UV-visible, FT-IR and theoretical approaches, *Colloids and Surfaces A* **611** (2021) 125810. https://doi.org/10.1016/j.colsurfa.2020.125810

[8] T. Laabaissi, F. Benhiba, M. Missioui, Z. Roui, M. Rbaa, H. Oudda, Y. Ramli, A. Guenbour, I. Warad, A. Zarrouk, Heliyon Coupling of chemical , electrochemical and theoretical approach to study the corrosion inhibition of mild steel by new quinoxaline compounds in 1 M HCl, *Heliyon* **6** (2020) e03939. https://doi.org/10.1016/j.heliyon.2020.e03939

[9] D. M. Mamand, T. M. K. Anwer, H. M. Qadr, Electronic structure and quantum chemical analysis of the corrosion inhibition efficiency of quinoxalines, *Journal of the Indian Chemical Society* **100** (2023) 101018. https://doi.org/10.1016/J.JICS.2023.101018

[10] Q. Deng, S. Jeschke, R. K. Mishra, S. Spicher, S. Darouich, E. Schreiner, P. Eiden, P. Deglmann, J. N. Gorges, X. B. Chen, P. Keil, I. Cole, Design of alkyl-substituted aminothiazoles to optimise corrosion inhibition for galvanised steel: A combined experimental and molecular modelling approach, *Corrosion Science* **227** (2024) 111733. https://doi.org/10.1016/j.corsci.2023.111733

[11] ASTM, Standard Practice for Preparing, Cleaning, and Evaluating Corrosion Test Specimens. Designation: G1-03, *ASTM Special Technical Publication* (2017) 505-510.

[12] F. Benhiba, Z. Benzekri, Y. Kerroum, N. Timoudan, R. Hsissou, A. Guenbour, M. Belfaquir, S. Boukhris, A. Bellaouchou, H. Oudda, A. Zarrouk, Assessment of inhibitory behavior of ethyl 5-cyano-4-(furan-2-yl)-2-methyl-6-oxo-1,4,5,6-tetrahydropyridine-3-carboxylate as a corrosion inhibitor for carbon steel in molar HCl: Theoretical approaches and experimental investigation, *Journal of the Indian Chemical Society* **100** (2023) 100916. https://doi.org/10.1016/j.jics.2023.100916

[13] A. Thoume, D. B. Left, A. Elmakssoudi, F. Benhiba, A. Zarrouk, N. Benzbiria, I. Warad, M. Dakir, M. Azzi, M. Zertoubi, Chalcone oxime derivatives as new inhibitors corrosion of carbon steel in 1 M HCl solution, *Journal of Molecular Liquids* **337** (2021) 116398. https://doi.org/10.1016/j.molliq.2021.116398

[14] R. G. Parr, W. Yang, Density Functional Approach to the Frontier-Electron Theory of Chemical Reactivity, *Journal of the American Chemical Society* **106** (1984) 4049-4050. https://doi.org/10.1021/ja00326a036

[15] H. Sun, Compass: An ab initio force-field optimized for condensed-phase applications - Overview with details on alkane and benzene compounds, *Journal of Physical Chemistry B* **102** (1998) 7338-7364. https:/doi.org/10.1021/jp980939v

[16] W. Sun, H. Wang, Moisture effect on nanostructure and adhesion energy of asphalt on aggregate surface: A molecular dynamics study, *Applied Surface Science* **510** (2020) 145435. https://doi.org/10.1016/j.apsusc.2020.145435

[17] M. El Faydy, F. Benhiba, N. Timoudan, B. Lakhrissi, I. Warad, S. Saoiabi, A. Guenbour, F. Bentiss, A. Zarrouk, Experimental and theoretical examinations of two quinolin-8-ol-piperazine derivatives as organic corrosion inhibitors for C35E steel in hydrochloric acid, *Journal of Molecular Liquids* **354** (2022) 118900. https://doi.org/10.1016/j.molliq.2022.118900

[18] W. L. Xu, X. Wang , G. A. Zhang, Efficient inhibition of mild steel corrosion in acidic medium by novel pyrimidine derivatives: Inhibitive effect evaluation and interface, *Journal of Molecular Structure* **1291** (2023) 136005. https://doi.org/10.1016/j.molstruc.2023.136005

[19] X. Liu, Y. Gao, J. Guan, Q. Zhang, Y. Lin, C. Shi, Y. Wang, J. Du, N. Ma, Corrosion inhibition properties of spinach extract on Q235 steel in a hydrochloric acid medium, *Arabian Journal of Chemistry* **16** (2023) 105066. https://doi.org/10.1016/j.arabjc.2023.105066

[20] Y. Qiang, L. Guo, H. Li, X. Lan, Fabrication of environmentally friendly Losartan potassium film for corrosion inhibition of mild steel in HCl medium, *Chemical Engineering Journal* **406** (2021) 126863. https://doi.org/10.1016/j.cej.2020.126863

[21] K. Raviprabha, R. S. Bhat, Corrosion inhibition of mild steel in 0.5 M HCL by substituted 1,3,4-oxadiazole, *Egyptian Journal of Petroleum* **32** (2023) 1-10. https://doi.org/10.1016/j.ejpe.2023.03.002

[22] X. Wang, W.L. Xu, Z.Y. Liu, G.A. Zhang, Unraveling the corrosion inhibition mechanism of triazine derivatives for carbon steel: Experimental and theoretical insights into interfacial adsorption, *Corrosion Science* **220** (2023) 111288. https://doi.org/10.1016/j.corsci.2023.111288

[23] A. Salhi, S. Tighadouini, M. El-Massaoudi, M. Elbelghiti, A. Bouyanzer, S. Radi, S. El Barkany, F. Bentiss, A. Zarrouk, Keto-enol heterocycles as new compounds of corrosion inhibitors for carbon steel in 1 M HCl: Weight loss, electrochemical and quantum chemical investigation, *Journal of Molecular Liquids* **248** (2017) 340-349. https://doi.org/10.1016/j.molliq.2017.10.040

[24] M. El Faydy, M. Galai, A. El Assyry, A. Tazouti, R. Touir, B. Lakhrissi, M. Ebn Touhami, A. Zarrouk, Experimental investigation on the corrosion inhibition of carbon steel by 5-(chloromethyl)-8-quinolinol hydrochloride in hydrochloric acid solution, *Journal of Molecular Liquids* **219** (2016) 396-404. https://doi.org/10.1016/j.molliq.2016.03.056

[25] A. Berrissoul, E. Loukili, N. Mechbal, F. Benhiba, A. Guenbour, B. Dikici, A. Zarrouk, A. Dafali, Journal of Colloid and Interface Science Anticorrosion effect of a green sustainable inhibitor on mild steel in hydrochloric acid, *Journal of Colloid and Interface Science* **580** (2020) 740-752. https://doi.org/10.1016/j.jcis.2020.07.073

[26] J. Lazrak, E. Ech-chihbi, B. El Ibrahimi, F. El Hajjaji, Z. Rais, M. Tachihante, M. Taleb, Colloids and Surfaces A : Physicochemical and Engineering Aspects Detailed DFT / MD simulation , surface analysis and electrochemical computer explorations of aldehyde derivatives for mild steel in 1 . 0 M HCl, *Colloids and Surfaces A* **632** (2022) 127822. https://doi.org/10.1016/j.colsurfa.2021.127822

[27] J. M. Frisch, G.W. Trucks, H. B. Schlegel, G. E. Scuseria, M. A. Robb, J. R. Cheeseman, G. Scalmani, V. B arone, B. Mennucci, G. A. Petersson, H. Nakatsuji, M. Caricato, X. Li, H. P. Hratchian, A. F. Izmaylov, J. Bloino, G. Zheng, J. L. Sonnenberg, M. Hada, G*AUSSIAN 09 Révision*., Gaussian, Inc., Wallingford CT,. (2009).

[28] K. S. Miled Ferigita, M. Saracoglu, M. G. Kadhim AlFalah, M. I. Yilmazer, Z. Kokbudak, S. Kaya, F. Kandemirli, Corrosion inhibition of mild steel in acidic media using new oxo-

pyrimidine derivatives: Experimental and theoretical insights, *Journal of Molecular Structure* **1284** (2023) 135361. https://doi.org/10.1016/j.molstruc.2023.135361

[29] T. H. El-Mokadem, A. I. Hashem, Nour E. A. Abd El-Sattar, E. A. Dawood, N. S. Abdelshaf, Green synthesis, electrochemical, DFT studies and MD simulation of novel synthesized thiourea derivatives on carbon steel corrosion inhibition in 1.0 M HCl, *Journal of Molecular Structure* **1274** (2023) 134567. https://doi.org/10.1016/j.molstruc.2022.134567

[30] M. El Faydy, F. Benhiba, I. Warad, S. Saoiabi, A. Alharbi, A. A. Alluhaybi, B. Lakhrissi, M. Abdallah, A. Zarrouk, Bisquinoline analogs as corrosion inhibitors for carbon steel in acidic electrolyte: Experimental, DFT, and molecular dynamics simulation approaches, *Journal of Molecular Structure* **1265** (2022) 133389. https://doi.org/10.1016/J.MOLSTRUC.2022.133389

[31] J. Saranya, F. Benhiba, N. Anusuya, R. Subbiah, A. Zarrouk, S. Chitra, Experimental and computational approaches on the pyran derivatives for acid corrosion, *Colloids and Surfaces A* **603** (2020) 125231. https://doi.org/10.1016/J.COLSURFA.2020.125231

[32] N. Anusuya, J. Saranya, P. Sounthari, A. Zarrouk, S. Chitra, Corrosion inhibition and adsorption behaviour of some bis-pyrimidine derivatives on mild steel in acidic medium, *Journal of Molecular Liquids* **225** (2017) 406-417. https://doi.org/10.1016/j.molliq.2016.11.015

[33] X. Yang, X. Lang, W. Dong, L. Yu, G. Chen, X. Li, Experimental and theoretical investigations on the inhibition of mild steel corrosion by capsaicin derivatives in hydrochloric acid, *Journal of Molecular Structure* **1283** (2023) 135341. https://doi.org/10.1016/j.molstruc.2023.135341